Amazon River influence on nitrogen fixation and export production in the Western Tropical North Atlantic

Sarah C. Weber[1], Edward J. Carpenter[2], Victoria J. Coles[3], Patricia L. Yager[4], Joaquim Goes[5], and Joseph P. Montoya[1]

[1] School of Biology, Georgia Institute of Technology, 311 Ferst Drive, Atlanta, GA, 30332, USA
[2] Romberg Tiburon Center, San Francisco State University, Tiburon, CA 94920 USA
[3] University of Maryland Center for Environmental Science, Horn Point Laboratory, Cambridge, MD 21613 USA
[4] School of Marine Programs, University of Georgia, Athens, GA 30602 USA
[5] Lamont-Doherty Earth Observatory, Columbia University, Palisades, NY 10964 USA

Abstract

As part of the multidisciplinary ANACONDAS program, we characterized the distributions of nutrients, particulate organic matter, phytoplankton, and stable carbon and nitrogen isotopes in the Amazon plume region during the spring high-flow period of May-June 2010. We encountered the lowest salinities (16.6 psu) near the southern end of our study region where the plume showed the greatest spatial coherence, and the highest salinities (36.0 psu) to the east of the plume. The major nutrients showed distinct patterns of variation with salinity, with NO_3^- largely absent from the surface plume and SiO_2 and PO_4^{3-} showing different degrees of conservative behavior. SiO_2 distributions were more strongly conservative, but with clear negative deviations that reflected biological consumption. In contrast, PO_4^{3-} concentrations showed clear positive deviations as large as 0.7 μM across a broad range of salinities as particle- and organically-bound P was released. These nutrient distributions resulted in strong nitrogen limitation and delivery of substantial amounts of SiO_2 and PO_4^{3-} to offshore waters, creating conditions that favored diazotrophy rather than simple eutrophication. We found a variety of diazotrophs in our study area, with interesting regional variation in their distributions. Mesohaline waters to the northwest of the plume axis were strongly dominated by Diatom-Diazotroph Associations (DDAs), particularly the *Hemiaulus hauckii – Richelia intracellularis* association. In contrast, *Trichodesmium* spp. were most abundant to the southeast of the plume. These two diazotrophs appeared to contribute to the nitrogen and carbon budgets of the upper water column in fundamentally different ways, with *H. hauckii* making a much greater contribution to the particulate nitrogen pool than *Trichodesmium* spp. (100% versus 50%, respectively), while contributing to a greater reduction in pCO_2 in the upper water column. These contrasts have important implications for the fate of new production, with DDAs supporting higher export flux than *Trichodesmium* spp. Our findings provide an important constraint on the role of the Amazon plume in creating distinct niches for diazotrophic phytoplankton, and for their role in the nutrient and carbon budgets of the Western Tropical North Atlantic.

Introduction

The Amazon River contributes nearly one fifth of the global riverine freshwater input into the ocean and is fed by the largest drainage basin in the world, encompassing nearly 6 million km^2 (Vorosmarty et al. 2000). The tremendous volume of water flowing from the Amazon forms a very dynamic and extensive surface plume that extends well offshore into the equatorial and tropical Atlantic Ocean. During the spring and summer months, the plume follows the North Brazil Current (NBC) along the northeastern coast of South America, carrying low salinity water to the Caribbean. In the fall and winter, the plume retroflects to the east as it becomes entrained in the North Equatorial Countercurrent (NECC). Early studies suggested that the primary impact of the Amazon plume on phytoplankton growth was constrained to coastal waters near the river mouth, with the large phytoplankton blooms in the retroflection supported primarily by local upwelling of nutrients (Longhurst 1993). Recent work in the Amazon plume and tropical Atlantic has begun to reveal the full extent of the Amazon River's influence on the Western Tropical North Atlantic (WTNA), including direct stimulation of primary production and nitrogen fixation hundreds of kilometers from the coast (Muller-Karger et al. 1995; Subramaniam et al. 2008).

The tropical North Atlantic was formerly considered a net source of CO_2 (~30 TgC y^{-1}; Takahashi et al. 2002; Mikaloff Fletcher et al. 2007) to the atmosphere, but new estimates of production supported by riverine nutrient inputs and diazotrophic (biologically fixed) nitrogen suggest that the western side of the basin may act as a net sink, sequestering ~28 TgC y^{-1} (Subramaniam et al. 2008). New nitrogen from diatom-diazotroph (N_2-fixer) associations (DDAs) and free-living N_2-fixers common in oligotrophic waters (*Trichodesmium* spp.) supports high rates of primary production throughout the plume region (Carpenter et al. 2004; Foster et al. 2007; Subramaniam et al. 2008). DDAs play an especially important role in ocean-atmosphere carbon exchange; as DDA blooms senesce or are consumed and defecated by zooplankton, their high silica content promotes rapid sinking through the water column. This process, referred to as the biological pump, results in the drawdown of atmospheric CO_2 and ultimately the sequestration of carbon in deep ocean sediments (Eppley & Peterson 1979; Gruber & Sarmiento 2002).

In order to better understand the mechanisms that drive biologically mediated carbon export in the WTNA, we embarked on a research cruise to the Amazon plume in spring 2010 as part of the multidisciplinary ANACONDAS program (Amazon iNfluence on the Atlantic: CarbOn export from Nitrogen fixed by DiAtom Symbioses). We used shipboard underway sampling and CTD-rosette systems to characterize over 450,000 km^2 of surface waters, generating high-resolution maps of nutrient concentrations and phytoplankton and stable isotope natural abundances. With these data we have better constrained the physical, chemical, and ecological properties of the Amazon plume system that stimulate diazotrophy and carbon export in the WTNA.

Material and Methods

Hydrographic Properties

Seawater and particle samples were collected on R/V *Knorr* cruise KN197-8 (May 22, 2010 – June 24, 2010) to the Amazon Plume region (Fig. 1a). We occupied a total of 25 stations along a cruise track that crossed the plume four times and extended well into offshore waters. Here, we focus on surface processes and have included only surface layer samples from CTD-rosette casts in our analyses. In addition to our hydrocasts, we used the shipboard underway seawater system to characterize hydrographic properties throughout the cruise. We also collected discrete samples from the underway seawater system at roughly hourly intervals while steaming between stations beginning with station 9 (3 June 2010) and continuing through the remainder of the cruise. Due to the delayed start of underway sample collection along our cruise track, none of our underway samples were obtained in fully oceanic waters, whereas surface CTD-rosette samples included the full salinity range we encountered on this cruise.

Seawater samples for nutrient analysis were collected directly (unfiltered) from the ship's seawater system or from the CTD-rosette. All of our nutrient samples (NO_3^-, PO_4^{3-}, SiO_2) were analyzed at sea using a Lachat QuickChem 8000 FIA system. We assessed the impact of conservative mixing of plume and offshore waters on nutrient distributions by performing a linear regression between averaged nutrient concentrations from waters with the lowest measured salinity (avg 17.95 psu) and from offshore oceanic stations (avg 35.62 psu) southeast of the plume (Table 1).

Suspended particles (e.g., phytoplankton, detritus) were collected by gentle pressure filtration of 2-18 L of seawater through pre-combusted (450° C for 2 h) 47-mm GF/F filters that were then dried at 60° C and stored over desiccant for analysis ashore.

Measurements of surface pCO_2 were made using an underway pCO_2 system (Sweeney et al. 2000) with a non-dispersive infrared CO_2 gas analyzer (LICOR 6252), and were standardized using CO_2-air reference gas mixtures from NOAA's Climate Monitoring and Diagnostics Laboratory. The precision of our pCO_2 measurements was ± 1 μatm. ΔpCO_2 (observed – atmosphere) was scaled to plume thickness (scaled-ΔpCO_2) by multiplying ΔpCO_2 by a plume thickness factor (ptf) reflecting the variations in plume thickness in our study area (Fig. 9).

Surface DIC samples were taken from the CTD-rosette, and analysis of samples from stations 14 – 22 is still in progress. Concentrations were measured on preserved samples using standard protocols (Cooley & Yager 2006) at the University of Georgia with a SOMMA/coulometer (Johnson et al. 1993; 1998) with ~0.5 μmol kg^{-1} precision. DIC measurements were checked for accuracy using Certified Reference Materials. Biological depletion of DIC (ΔDIC_{BIO}) was calculated using methods from Cooley & Yager (2006). We used trapezoidal integration of multiple CTD-rosette samples located within the plume to estimate the areal impact of biological uptake of DIC. Integrated ΔDIC_{BIO} is reported here as $\Delta DIC_{BIO,INT}$.

Phytoplankton Community

Samples for phytoplankton enumeration were collected by gently filtering 2 - 4 L of seawater from the flow-through system or the CTD-rosette through 20 μm Nitex mesh. The samples were gently backwashed off the mesh with about 50 mL of filtered seawater and then fixed with acidic Lugol's solution. A well-mixed 15 mL aliquot from this tube was then centrifuged at 2000 rpm for 20 minutes and 14 mL of supernatant was drawn off. The cells within the remaining 1 mL were resuspended and were placed in a Sedgwick-Rafter counting chamber. Transects were then counted at 320X using a long working distance objective on a Zeiss Axioskop microscope.

An Advanced Laser Fluorometer (ALF), which is capable of distinguishing multiple phytoplankton pigments, was connected to the ship's uncontaminated seawater flow-through system on all transits between stations. Using the ALF in conjunction with other instruments allowed for continuous measurements of salinity, temperature, and fluorometric Chl *a* in water from approximately 5 m below the surface along the cruise track shown in Fig. 1. With the exception of a few breaks for reconditioning, the ALF was operated throughout the cruise, providing near-real time distribution patterns of hydrographic, chemical, and biological properties over a distance of 700 km inside and outside the plume.

Elemental and Isotopic Analyses

All elemental concentration and stable isotope natural abundance measurements were made by continuous-flow isotope-ratio mass spectrometry (CF-IRMS) using a Micromass Optima interfaced to a CE NA1100 elemental analyzer for online combustion and purification of sample nitrogen and carbon. All stable isotope abundances are reported as $\delta^{15}N$ and $\delta^{13}C$ values relative to atmospheric N_2 and VPDB, respectively. Each analytical run included a size series of

elemental (acetanilide or methionine) and isotopic (peptone) standards, which provided a check on the stability of the instrument and allowed us to remove the contribution of any analytical blank from our isotopic measurements (Montoya 2008). We conservatively estimate that the overall analytical precision of our isotopic measurements is better than ±0.1‰.

Isotope Mixing Model

Diazotroph nitrogen (N_D) contribution to suspended particles was calculated using the nitrogen isotope mass balance approach (Montoya et al. 2002). Two major sources of allochthonous nitrogen influence surface waters in the plume after riverine nitrogen has been fully consumed: a.) nitrogen fixed by diazotrophs in contrast to b.) NO_3^- mixed or upwelled from below along with N transported in organic form in the plume itself. In our system, these two sources (diazotroph N vs NO_3^- + organic N) show a strong isotopic contrast, which we exploited to calculate N_D by partitioning the contribution of subsurface/riverine NO_3^- + organic N and biological N_2-fixation to suspended particles as

$$N_D(\%\ \text{Diazotroph N}) = 100 \times \frac{\delta^{15}\text{N}_{\text{particles}} - \delta^{15}\text{N}_{\text{Nitrate + organic N}}}{\delta^{15}\text{N}_{\text{diazotroph}} - \delta^{15}\text{N}_{\text{Nitrate + organic N}}} \qquad (1)$$

where $\delta^{15}N(NO_3^-$ + Organic N) = 5‰ and $\delta^{15}N_{diazotrophs}$ = -2‰. We used $\delta^{15}N(NO_3^-$ + Organic N) = 5‰ because this value is characteristic of the southern end of our survey area and likely reflects a combination of N derived from the Amazon River and Atlantic deep-water NO_3^- (4.5‰; Sigman et al. 2000). The $\delta^{15}N_{diazotrophs}$ value of -2‰ is characteristic of diazotrophic biomass (Montoya et al. 2002).

Results

Hydrographic Properties

Surface waters (0-5m) ranged in salinity between 16 and 37 psu and in temperature between 28 and 30.5˚C, with the lower temperatures corresponding to fresher water. We defined plume regions based on salinity following the convention of Subramaniam et al. (2008): "low salinity" waters with S < 30 psu; "mesohaline" with S = 30-35 psu; and "oceanic" waters with S > 35 psu. Salinity tended to decrease northward along the plume axis, but with appreciable local variability within this general trend (Fig. 2a, c). Within the low salinity plume core between roughly 5 and 7˚N, surface salinity first dropped from ~21 psu to the lowest measured salinity of ~16 psu at 6˚N before increasing again to ~19 psu by 6.5˚N. Farther to the northwest was another region of low salinity plume water, which gradually decreased in salinity from 23.5 to 27.7 psu between 9.5 and 12.5˚N.

Plume thickness and width tended to increase in magnitude with distance along the plume axis, reflecting increased mixing with oceanic water and physical dispersal. Plume thickness remained fairly constant in the low salinity plume core, ranging between 4 – 6 m (data not shown). Elsewhere, the physical properties of the plume could vary quite substantially on a time scale of a few hours, with the most dramatic changes taking place near the plume edges. For example, between two CTD-rosette casts 1.5 h apart in the same location at station 23 (10.6˚N 54.4˚W), plume thickness decreased from 12 to 5 m while surface salinity remained at 26.5 psu. At station 9 (6.1˚N 50.9˚W), plume thickness gradually increased from 7 to 22 m over a 35 h period before decreasing sharply to 5 m in just 1.5 h. Salinity dropped from 34.2 to 29.0 an hour prior to the decrease in plume thickness.

The dynamic nature of the plume is also evident in comparisons of measurements taken in regions of overlap between legs 1 and 2 of the cruise. There were two particularly interesting areas of overlap at around 6 – 7 and 9 – 13˚N. These areas were first sampled on May 24 and 27, respectively, and then again on June 8 – 10 and June 14 – 16, resulting in a ca. 16 day gap between measurements in the southern area of overlap, and a ca. 20 day gap to the north. On leg 1 between 6 – 7˚N, the plume was ~5 psu saltier, contained ~0.2 – 0.5 RFU less of chl *a,* and was much farther to the southwest compared to leg 2. In the northern area between 9 – 13˚N, we saw much less plume influence with again a difference of ~5 psu. There was also a very large shift in

chl *a* concentrations and distributions. On leg 1, we encountered a small bloom between 54 – 55˚W, and very low chl *a* (< 0.2 RFU) to the west of this feature. Some 20+ days later, the region west of 55˚W was characterized by an extensive feature of elevated chl *a* (0.4 – 0.9 RFU), with very low biomass to the east. Unfortunately, further comparisons of biological and chemical characteristics of the plume between the two cruise legs cannot be made since the full suite of underway measurements was not started until leg 2.

Nutrient Distributions

Nitrate was mostly absent from surface waters, with only occasionally measurable concentrations distributed across the three salinity regions (Fig. 3a). The maximal value of 0.60 μmol L^{-1} (μM) was located in low salinity plume waters (18.4 psu) at 6˚N 51.5˚W (Fig. 4b).

Phosphate concentrations generally decreased with increasing salinity ($r = -0.342$, $p \leq 0.0001$), ranging from 0.03 to 0.55 μM along the conservative mixing line, but with very strong positive deviations in all salinity regions (Figs. 3b, 4c). These deviations were most pronounced in low salinity waters, where the magnitude of the deviations increased with distance along the plume axis (Fig. 4e).

Silicate concentrations ranged from 0.37 to 49.80 μM and showed generally conservative behavior as a function of salinity ($r = -0.958$, $p \leq 0.0001$; Figs. 3c, 4d), though many stations exhibited marked departures from the conservative mixing line in the low salinity and mesohaline regions (Fig. 4f). These anomalies were almost exclusively negative, reflecting a deficit of SiO_2 relative to expectation.

Elemental and Isotopic Distributions

Particulate carbon and nitrogen (PC and PN) concentrations showed similar distributions relative to salinity, with the highest concentrations (126.9 μM C, 10.5 μM N) at the southernmost part of the plume that we sampled (Figs. 5c, d). These elevated values did not coincide with the lowest salinity waters due to the local salinity variation mentioned above. The C and N concentrations then dropped sharply at 5.5˚N to ~19 and ~2 μM, respectively, and remained at or slightly below these levels to the northeast and at the western parts of our cruise track across the northern plume. On one of these western transects, at 11.3˚N and 56.0 – 56.8˚W, both C and N were present at concentrations comparable to those in the southern plume

(16.2 – 46.2 μM C; 1.4 – 3.1 μM N). Concentrations ranged between 2.0 – 5.0 μM C and 0.3 – 1.0 μM N everywhere else.

C:N ratios did not follow a monotonic relationship relative to salinity (Fig. 5b). The ratios were highest in the near-shore, low salinity plume (9 – 16) and in the mesohaline waters (9 – 11) west of the northern plume. There were also two prominent areas along our cruise track characterized by low C:N ratios of 4.5 – 6.6, (below Redfield stoichiometry). The largest feature extended from the southern plume core north into mesohaline waters between 6 and 9˚N, where C and N concentrations were still slightly elevated (5.0 – 10.0 μM C; 1.0 – 2.2 μM N). The second, smaller feature with high C and N was offset to the east of the northern plume between 11.5 and 12.5˚N.

The $\delta^{15}N$ of particles ranged between -4.6 and 6.4‰ (Fig. 6c) and showed a general decrease with increasing salinity, except in 17 – 21 psu waters between 6 – 7˚N (Fig. 7b), where $\delta^{15}N$ increased from 1.9 to 4.5‰. $\delta^{15}N$ was highest in the southern, low salinity plume and became more variable with increasing salinity, but tended to decrease in the mesohaline region, approaching low values typical of diazotrophic biomass (ca. -2‰; Montoya et al. 2002). Spatially, these low $\delta^{15}N$ values were located at both the eastern and western edges of the northern plume, with the most negative feature overlapping with the high C and N waters at about 11.5˚N 56˚W. The other low $\delta^{15}N$ feature was to the east of the plume at 12.5˚N and between 52 and 54.5˚W.

The $\delta^{13}C$ of suspended particles ranged from -23.7 to -14.6‰ and showed greater variation with salinity than we observed for the nitrogen isotopes (Fig. 6b). Variation in $\delta^{13}C$ was greater, though positively skewed, in the mesohaline region of the plume, due to a western bias toward high $\delta^{13}C$. These mesohaline waters west of the plume were characterized by an expansive region of elevated $\delta^{13}C$ (Fig. 7c), which also contained the highest values measured (-18.0 to -14.6‰). Only two small patches of comparably high values were present east of the plume at 12.5˚N 53˚W, and 9˚N 50.5˚W.

Phytoplankton Distributions

Chlorophyll *a* concentrations were highest (6.0 – 11.0 RFU) in the southernmost plume core between 5 – 5.5˚N and decreased down to 1.0 RFU to the north up to 6.5˚N (Figs. 2b, d). There

was more chl *a* in the western mesohaline waters (0.5 – 0.8 RFU) than to the east and everywhere else, where concentrations ranged from the limit of detection to 0.3 RFU.

Trichodesmium spp. and DDAs, primarily *Hemiaulus hauckii* and *Rhizosolenia clevei*, were most abundant in mesohaline waters of the outer plume regions. *H. hauckii* was the dominant diazotroph host, with the highest cell count exceeding 9.6×10^5 cells L^{-1} at 9.7˚N 55.5˚W (Figs. 6a, 8a). The majority of *H. hauckii* biomass was to the west of the plume, though two smaller blooms were present to the east. This spatial distribution of *H. hauckii* correlated very closely with elevated $\delta^{13}C$ (0.4Figs. 8a, 7b). Though *H. hauckii* was most abundant in mesohaline regions, it was still present in significant concentrations ($2.6\times10^4 – 5.7\times10^3$ cells L^{-1}) in the northern low salinity plume between 10 and 12˚N, but not above this latitude.

R. clevei were far less abundant, with maximum concentrations barely surpassing 800 cells L^{-1} (Figs. 6a, 8c). *R. clevei* was mostly confined to the northernmost mesohaline waters above 11˚N and was slightly more abundant on the eastern side of the plume. There was also a small bloom (< 320 cells L^{-1}) in the mesohaline waters to the east of the southern plume core.

Trichodesmium spp. were broadly distributed and present in significant abundance, but at concentrations much lower than *H. hauckii.* Trichome counts reached 2.0×10^3 trichomes L^{-1}, with a maximum of 3.6×10^3 trichomes L^{-1} at 6˚N 51˚W, east of the southern plume (Figs. 6a, 8d). The biomass of *H. hauckii* and *Trichodesmium* spp. can be compared by assuming that one *Trichodesmium* spp. trichome contains about an order of magnitude more carbon than an individual *H. hauckii* cell. With these assumptions, *H. hauckii* biomass was usually 10 – 20 times greater than that of *Trichodesmium spp.* (data not shown). In general terms, *Trichodesmium spp.* abundance increased on the plume periphery from north to south, with higher concentrations east of the plume, which was opposite of the trend we saw for *H. hauckii*

Sources of Nitrogen

We used a linear isotopic mixing model (Eqn. 1) to calculate the relative contributions of subsurface nitrate and N_2-fixation to the particulate nitrogen pool (Montoya et al. 2002). We found that the diazotrophic contribution to nitrogen (% N_D) increased in magnitude and variability with increasing salinity, with broad areas of 100% N_D in the mesohaline and oceanic regions of our cruise track (Fig. 7d). The diazotrophic contribution to particles correlated closely with *H. hauckii* concentration (Figs 8b), was generally ≥ 80% N_D at all *H. hauckii* bloom locations, and was at or near 100% N_D where both *H. hauckii* and *Trichodesmium spp.* were

present in high abundances (9 and 12.5˚N to the east of the plume and 11.5˚N to the west; Figs. 8b, 8d). At the largest *Trichodesmium spp.* bloom near 6˚N, 51˚W (Fig. 8d), the diazotrophic contribution was only ~50% N_D, similar to what we observed in surrounding waters (Fig. 7d).

DIC and pCO_2

Surface pCO_2 concentrations showed a direct relationship with salinity, ranging from 100 µatm in low salinity waters to 500 µatm in oceanic regions, though pCO_2 varied by as much as 200 µatm over most of the salinity range. Some of the variation in mesohaline waters can be attributed to the occurrence of spatially distinct water masses with similar salinities but different pCO_2 concentrations. There are two areas on either side of the southern plume core whose salinities fell in the mesohaline range, but the pCO_2 in these areas was much higher (420 – 480 µatm) relative to the mesohaline waters to the north (290 – 400 µatm). There was also a clear east-west gradient in pCO_2 in the northern region of our survey area. In general, pCO_2 was highest to the east at roughly 400 µatm, and dropped to 300 µatm within the northern plume, before rising slightly to 350 µatm on the western side.

Depletion relative to atmosphere (ΔpCO_2) was most prominent in the low salinity southern plume core, ranging between -220 and -300 µatm at salinities of 20 – 21.5 psu. The thickness of the surface plume varied by 4- to 6-fold, so we scaled the absolute CO_2 deficit in the surface layer by the thickness of the plume to assess the overall drawdown of CO_2 in the surface layer (scaled-ΔpCO_2). The spatial distribution of scaled-ΔpCO_2 (Fig. 9) revealed that the magnitude of pCO_2 depletion in northern mesohaline waters is comparable to that in the southern plume core.

Surface DIC concentrations showed a strong positive relationship with salinity, with 1170 µmol kg^{-1} in the low salinity plume (20 psu) and 2000 µmol kg^{-1} at 36 psu. DIC drawdown in surface samples due to biological activity (ΔDIC_{BIO}) was twice as great in the southern plume core as in the northwestern mesohaline region (100 vs 50 µmol kg^{-1}). When we integrated ΔDIC_{BIO} through the plume layer ($\Delta DIC_{BIO,INT}$; Fig. 9), we found that the northwestern mesohaline region actually experienced more biological DIC drawdown (860 – 980 mmol m^{-2}) than the southern plume (630 – 700 mmol m^{-2}). Over our entire survey region, mesohaline and oceanic waters to the east of the southern plume core showed the lowest biological contribution to DIC drawdown.

Discussion

The ANACONDAS program builds on previous studies that have characterized the physical (Longhurst 1993; Muller-Karger et al. 1995), biogeochemical (Demaster et al. 1986; Fox 1989; Demaster & Pope 1996; Subramaniam et al. 2008; Yeung et al. 2012; Goes et al. Submitted), and ecological (Smith & Russell 1995; Smith & Demaster 1996; Foster et al. 2007; Subramaniam et al. 2008; Goes et al. Submitted) nature of the Amazon River plume. Our study provides a comprehensive overview of nutrient and particle dynamics in the Amazon plume system during the spring high-flow season, when the plume extends to the northwest and transports surface water to the Caribbean. We documented the highly dynamic nature of the Amazon plume system and explored its potential impacts on coastal and offshore waters of the Western Tropical North Atlantic.

Our underway data and kd490 composite satellite images (Figs. 1c, 2c) both show that the plume was narrow and coherent in the southern reaches of our cruise track, and broadened and dispersed to the north along the plume axis. We also saw sharper gradients to higher salinity waters to the east of the northern plume, whereas the western region showed more evidence of lateral mixing and a lower overall salinity. These regional differences in the physical structure of the plume have important implications for the distribution of nutrients as well as functionally diverse phytoplankton communities and their contributions to nutrient and carbon cycling in the upper water column.

The strongly river-influenced core of the southern plume varied in salinity by as much as 5 psu, with no clear directional trends. The thickness of the low-salinity surface plume in this region was 4 – 6 m, creating the potential for the R/V *Knorr's* underway-sampling system, with an intake ~4.5 m below the sea surface, to collect water from beneath the plume layer. This seems to have occurred at low frequency, though, since surface samples from 20 CTD-rosette casts (stations 10 – 18) that sampled within the plume (3 – 4m) throughout this region, are in good agreement with the UW physical data, which validates our observations of strong local salinity variability. The episodic nature of the plume is further highlighted through the comparison of plume locations and physical properties between cruise legs 1 and 2, giving us some sense of change through time. Even though coverage on leg 1 is minimal, it appears that a bolus of very low salinity plume water pulsed into the southern region of our survey area within

the span of 16 days, shifting the plume core farther northwest. The plume's influence also greatly increased to the northwest, as it appears that the northern section of the plume moved much farther to the west within a similar time span, and was accompanied by a large decrease in scaled-pCO_2 (-15 vs -150 µatm) and a large increase in $DIC_{BIO,INT}$ (-140 vs 900 mmol m^{-2}). We also found similar contrasts between legs 1 and 2 in the southern end of our work area (-90 vs -230 µatm and 430 vs 560 mmol m^{-2}, respectively). These observations provide strong evidence of the episodic and dynamic nature of the plume, which creates a patchwork of waters of varying age, physical properties, and biological impact.

Nutrient and Phytoplankton Distributions

Nutrient concentrations (NO_3^-, PO_4^{3-}, and SiO_2) showed marked departures from conservative mixing between riverine and oceanic waters. Nitrate was mostly absent from surface waters along our cruise track (Fig. 4b), in keeping with the results of previous studies (Smith & Russell 1995; Demaster & Pope 1996; Smith & Demaster 1996), with only a few instances of measurable NO_3^- in the southern plume core. Phosphate had a much more complicated distribution relative to salinity, with strong deviations from conservative mixing in all salinity regions (Figs. 3b, 4e). We found evidence of PO_4^{3-} drawdown in the southern plume, though it appears that conservative mixing was the primary factor in shaping PO_4^{3-} distributions below 9˚N, since PO_4^{3-} deviations remained close to zero across steep salinity gradients at 7.5˚N (Fig. 4e). Phosphate concentrations increased substantially to the north along the plume axis, leading to strong positive deviations from conservative mixing. This trend can be explained by the release of PO_4^{3-} from suspended particles within the surface plume, as previously described by Fox et al. (1986) and Berner & Rao (1994). Silicate exhibited the most nearly conservative behavior relative to salinity ($r = -0.958$, $p \leq 0.001$; Fig. 3c), but nonetheless showed considerable negative deviations over most of our cruise track and across all salinity regions (Fig. 4f). Negative SiO_2 deviations were prominent on the western side of the plume, where the large diatom *H. hauckii* was the most abundant ($r = -0.229$, $p = 0.0003$), but did not significantly correlate with *R. clevei* ($r = -0.061$, $p = 0.399$) or *Trichodesmium* spp. ($r = 0.032$, $p = 0.674$) abundances. There were also substantial negative deviations in SiO_2 concentration in the southern plume waters, where coastal diatom species dominated the biomass.

The conservative mixing line we calculated for SiO_2 (slope = -2.77 µM psu^{-1}; ordinal intercept = 100 µM) was in close agreement with that of Yeung et al. (2012), who calculated a

slope of -2.45 μM psu^{-1} and an extrapolated river end-member (0 psu) concentration of 89 μM. These SiO_2 mixing lines appear to produce conservative estimates of river end-member SiO_2 concentrations relative to a previous study conducted by DeMaster et al. (1996), who extrapolated a freshwater value of 144 μM from measurements taken in water with salinities between 5 – 10 psu. Our PO_4^{3-} conservative mixing line produced a higher PO_4^{3-} river end-member value (1.0 μM) than the DeMaster et al. (1996) value of 0.7 μM. The release of PO_4^{3-} from suspended particles and/or dissolved organic matter complicates nutrient dynamics, making it difficult for either study to accurately extrapolate to the river end-member. Due to the lack of actual river end-member data in our study, we cannot confidently anchor our SiO_2 and PO_4^{3-} mixing lines in 0 psu waters, as we cannot account for consumption/remineralization processes up-stream of our sampling area or for seasonal variability in riverine nutrient concentrations. On the other hand, SiO_2 and PO_4^{3-} measurements from the low salinity southern regions of our survey area provide a robust end-member for our work, which focuses primarily on offshore waters and processes.

The ambient nutrient concentrations within the surface waters of the plume were all far below the Redfield N:P ratio of 16:1, implying severe nitrogen limitation of the phytoplankton. In addition, Si:P was mostly below the Redfield-Brzezinski value of 15:1 (1985), with the exception of five small patches on the plume periphery in mesohaline and oceanic waters to both the east and west. *H. hauckii* was more closely associated with near-Redfield-Brzezinski Si:P regions than were Trichodes*mium spp.* (Fig. 9), suggesting that *H. hauckii* blooms are strongly dependent on the relative concentrations of SiO_2 and PO_4^{3-}, while the abundance of *Trichodesmium* spp. was regulated primarily by PO_4^{3-} availability. These differences in nutrient requirements are likely one of the main drivers of the strong spatial variations we observed in the abundance of the major phytoplankton groups, and the distribution of nutrients clearly favored the growth of nitrogen fixers in offshore waters. The aging plume can act as a powerful stimulant of diazotrophy through the delivery of PO_4^{3-} from particles to the SiO_2-rich, NO_3^--poor mesohaline waters to the north. In facilitating diazotrophy far offshore, this PO_4^{3-} transport mechanism plays a crucial role in promoting the biological export of carbon to the deep ocean. This enhancement of the biological pump has important implications for the regional carbon budget and may be an important factor in other tropical river-ocean systems (e.g, the Congo and Mekong Rivers).

Phytoplankton distributions showed distinct north/south and east/west trends as well as clear evidence of niche partitioning among diazotrophs (N_2-fixers). Of the diazotrophic phytoplankton examined in this study, *H. hauckii* DDAs were by far the most numerically abundant (Fig. 6a), dominating the northwestern mesohaline waters. In contrast, *Trichodesmium spp.* concentrations were highest in mesohaline and oceanic waters to the southeast of the plume (Figs. 6a, 8d). On close inspection, *H. hauckii* was almost always present in locations where we found *Trichodesmium* spp., though *Trichodesmium* spp. usually occurred in higher concentrations when *H. hauckii* was in very low abundance. These distributions may be a reflection of competition between the two diazotrophs, as *H. hauckii* has a higher intrinsic growth rate than *Trichodesmium* spp. (Foster et al. 2007), but *Trichodesmium* spp. are known to produce a variety of allelopathic compounds capable of inhibiting competitors and predators (Hawser et al. 1992; Capone 2005). *H. hauckii* is also known to directly outcompete *R. clevei*, possibly due to *H. hauckii*'s comparatively smaller size (with implications for nutrient uptake; Foster et al. 2007), faster growth rate (Villareal 1989; Villareal 1990), or symbiont availability (Foster et al. 2007), all of which may have contributed to the very low abundances of *R. clevei* we observed in our samples (Figs. 6a, 8c).

Particulate Organic Matter & Stable Isotopes

Particulate carbon and nitrogen concentrations were relatively high in the southernmost part of our sampling region (Figs. 5c, d), which contained the youngest plume waters, suggesting that at least some of the high particle load may have originated from the Amazon River itself. Organic particle concentrations then dropped by an order of magnitude just to the north of this region within the low salinity waters. We also saw slightly elevated C and N concentrations in the northwestern mesohaline waters, corresponding with regions of high *H. hauckii* abundance (Fig. 8b). These high concentrations reflect the ability of rapidly growing diatoms to produce biomass when nutrients (in this case, Si and P) are available, which in turn provides an important source of organic matter to support the pelagic food web as well as vertical transport to depth. The atomic ratio of C to N in particles was usually above the Redfield ratio of 6.6 in areas with high phytoplankton biomass (Figs. 5b, 8b, d), most notably in the far southern and northwestern regions. This is consistent with the strong nitrogen limitation implied by our nutrient measurements as well as our direct rate measurements (discussed elsewhere) and integrative estimates of N_2-fixation derived from isotope budgets.

Our measurements of the natural abundance of ^{13}C and ^{15}N in organic particles provided us with an integrative measure of the major processes influencing C and N cycling in the Amazon plume region. The variation in C isotopes in our data appears to be strongly influenced by large, rapidly growing diatoms, in which CO_2-fixation tends to become diffusion limited, leading to limited expression of the enzymatic fractionation of carbon isotopes and high $\delta^{13}C$ values in the organic matter formed (Goericke et al. 1994; Laws et al. 1995; Rau et al. 1996). In our data, elevated $\delta^{13}C$ values in organic matter matched very well to *H. hauckii* blooms ($r = 0.470$, $p \leq 0.001$; Figs. 7b, 8b), in keeping with the effects of size and growth rate on carbon isotopic fractionation.

While C isotopes reflect phytoplankton size and growth rate, N isotopes provide a good index for N_2-fixation, with lower $\delta^{15}N$ values indicative of N derived from diazotrophy. Using our isotope mixing model (Eq. 1), we were able to quantify the relative contribution of biologically fixed N to the particulate N pool (% N_D; Fig. 7). Diazotrophic contributions were near 100% in the northern mesohaline waters (Fig. 7d), and interestingly, these maxima in % N_D tended to co-occur with high abundances of *H. hauckii* ($r = 0.377$, $p \leq 0.001$), while the densest *Trichodesmium* spp. populations were associated with % N_D values of only ~50% ($r = 0.130$, $p = 0.061$; Fig. 10). This may partly reflect the difference in maximal population densities, which will limit the potential contribution of diazotroph N to the particle field, but trophic processes may also play an important role in generating this contrast. Carpenter et al. (1999) argued that nitrogen fixed by DDAs can readily enter the food web through direct grazing, in contrast to nitrogen fixed by *Trichodesmium* spp., which are grazed by only a small number of zooplankton species. The low $\delta^{15}N$ of particles associated with *H. hauckii* suggests that diazotrophic N is also likely retained in the upper water column as detritus and as rapidly recycled excreta (especially NH_4^+). Such remineralization processes and NH_4^+ recycling may explain the low values of $\delta^{15}N$ close to -3‰ (Fig. 6c; Montoya et al. 2002), which are more depleted in ^{15}N than our diazotrophic end-member.

DIC and pCO_2

Surface concentrations of pCO_2 and DIC provide insight into the role of biological processes on the carbon cycle in the WTNA. The distributions of pCO_2 depletion and biological DIC drawdown in our study area were closely associated with coastal diatoms and *H. hauckii*,

suggesting that these phytoplankton play a key role in shaping carbon cycle dynamics. When ΔpCO_2 was scaled to plume depth, these two phytoplankton groups appeared to have comparable impacts on regional pCO_2 depletion. *H. hauckii*'s relative influence on carbon export becomes more apparent when comparing ΔDIC_{BIO} integrated through the plume layer between these two regions. Areas to the northwest, which contained the largest *H. hauckii* blooms we encountered, showed the greatest $\Delta DIC_{BIO,INT}$, even higher than the southern plume. Interestingly, *Trichodesmium* spp. seemed to have little impact on either pCO_2 or DIC drawdown. The disparity in the magnitude of DIC and pCO_2 drawdown between regions associated with *H. hauckii* or *Trichodesmium* spp. is likely a reflection of differential export efficiencies of carbon to depth resulting from dissimilar food web interactions.

Regional Variations

Our data provide clear evidence for regional differentiation of the Amazon plume, with three distinct regions in the spring plume system that are characterized by different biogeochemical and ecological features. In brief, our sampling area can be divided into southern, northwestern, and northeastern regions. The southernmost region (below 8˚N), which we assume contains the youngest plume waters we encountered on our cruise, was a low salinity, low diazotrophy area. Despite extremely high chlorophyll *a* concentrations, diazotrophs were largely absent and the nutrient budget appeared to be dominated by riverine and deepwater sources, a characteristic that is reflected in the high $\delta^{15}N$, low N_D signature of particulate N. The southern plume was shallow and exhibited sharp horizontal gradients in salinity and SiO_2, indicating a limited impact of mixing with oceanic waters. SiO_2 and PO_4^{3-} were present in high absolute concentrations, but showed a deficit relative to conservative mixing as a result of consumption by coastal phytoplankton. With no NO_3^- in the surface waters, these coastal species, composed primarily of diatoms (Goes et al. Submitted), must have been rapidly drawing down all surface NO_3^- (Demaster & Pope 1996), producing an N-limited environment. It appears that the phytoplankton communities were in part sustained by subsurface NO_3^- from nearby upwelling at the shelf break (Goes et al. Submitted), and contributed to carbon export through classic eutrophication processes (Eppley & Peterson 1979; Lohrenz et al. 1997).

Moving north along the plume axis, we encountered increasingly salty and less spatially coherent plume waters, reflecting the impact of lateral and vertical mixing. Within the plume proper, PO_4^{3-} concentrations increased to the north due to release of P from particles and/or

dissolved organic matter, where as SiO_2 concentrations decreased due to mixing and consumption, but were still present in appreciable concentrations. The combination of river-derived SiO_2 and PO_4^{3-} released from particles far offshore in the absence of surface NO_3^- created a niche strongly favorable for nitrogen fixers.

To the east of the northern plume, steep salinity and SiO_2 gradients persisted, with relatively sharp transitions to oceanic water. In contrast, the plume dissipated more gradually into mesohaline waters in the northwestern region, where a physical-biological model suggests that mixing by mesoscale eddies was more prevalent (Coles, unpublished data). The western plume boundary was clearly dominated by *H. hauckii*, which was strongly associated with waters with lower Si:P ratios, likely as a result of the Si consumption associated with its (*H. hauckii*) production. The dynamic eddy features in this area may also play an important role in re-fertilizing the western region with SiO_2 and PO_4^{3-}, further stimulating the growth of this DDA.

The northeast region of our study area had lower abundances of *H. hauckii* and some small blooms of *Trichodesmium* spp., which were mostly absent in the west. *Trichodesmium* spp. were present in their highest abundances farther southeast, where plume influence was minimal. Although the distributions of *H. hauckii* and *Trichodesmium* spp. overlapped broadly, the highest abundances of the two diazotrophs were spatially distinct, with important implications for the regional biogeochemistry of the Western Tropical North Atlantic since the two diazotrophs appear to make different contributions of N to the rest of the ecosystem.

The overall distribution of diazotrophs during this high-flow period when the plume's influence extended well to the northwest, was highly associated with the plume boundaries. The spatial distribution of DDAs strongly affected the biogeochemistry of offshore waters, especially to the west of the plume, where blooms of *H. hauckii* were strongly associated with increased PN and PC, higher C:N ratios, higher $\delta^{13}C$, lower $\delta^{15}N$, and higher % N_D. This region also showed pCO_2 depletion comparable to the coastal diatom-dominated southern plume and even greater water column DIC drawdown. Taken together, these data provide strong evidcnce of the major regional impact of *H. hauckii* on the nitrogen and carbon cycles of the Western Tropical North Atlantic.

Conclusions

As part of the multidisciplinary ANACONDAS program, we characterized the distributions of nutrients, particulate organic matter, phytoplankton, and stable carbon and nitrogen isotopes in the Amazon plume region during the spring high-flow period. Our data provide an integrative overview of the impact of the plume on nutrient and elemental cycling as well as the distribution of major groups of diazotrophs. We found clear evidence that the Amazon plume plays a critical role in fertilizing offshore waters, but in a way that promotes diazotrophic growth rather than simple eutrophication. The diazotroph community itself showed interesting regional variation, with strong dominance by DDAs, primarily *H. hauckii*, in the mesohaline waters to the northwest of the plume axis. Our isotope budgets show that the two major diazotrophs in our study area, DDAs and *Trichodesmium* spp., contribute to the food web and to the vertical flux of organic matter in very different ways, though both are significant sources of new production in the plume. Specifically, DDAs appear to make a more direct contribution to the food web, which results in a much greater contribution to the overall export flux of carbon in this region, as surface waters associated with DDA blooms are highly depleted in DIC.

Recent studies have shown that the Western Tropical North Atlantic is a net sink, rather than a source for atmospheric CO_2 (Subramaniam et al. 2008) and our findings provide critical insight into the processes and organisms that are driving the removal of CO_2 from the upper water column. Specifically, the Amazon plume is stimulating growth of diazotrophic *H. hauckii*, DDAs whose carbon and nitrogen fixation is clearly contributing to the particle field and to the export of organic matter through the activity of the biological pump.

Although our work is specific to the Amazon plume region, the limited data available suggest that our findings are relevant to other large river systems that drain into tropical oceans, particularly the Congo (Foster et al. 2009) and the Mekong (Voss et al. 2006). In these and other systems, riverine inputs of nutrients and the processing of nutrients that occurs in the river plume, are likely to promote both diazotrophic activity and consumption of CO_2, with important impacts on the regional and global nutrient and carbon budgets.

Acknowledgements

I would like to thank the officers and crew of the R/V *Knorr* for their assistance and support in our work at sea, as well as Jason Landrum, Rachel Horak, Julia Grosse, and Julie Gonzalez for their assistance at sea and in the laboratory. I also thank Annalisa Bracco for her comments and Joe Montoya for his endless support. This research was supported by the grant NSF-ETBC-0934025 (JPM). SCW received partial support from the President's Undergraduate Research Program at Georgia Tech and from an REU supplement to NSF-ETBC-0934025.

References

Berner, R. A. and J. L. Rao (1994). "Phosphorus in Sediments of the Amazon River and Estuary - Implications for the Global Flux of Phosphorus to the Sea." Geochimica Et Cosmochimica Acta **58**(10): 2333-2339.

Brzezinski, M. A. (1985). "The Si-C-N Ratio of Marine Diatoms - Interspecific Variability and the Effect of Some Environmental Variables." Journal of Phycology **21**(3): 347-357.

Capone, D. G. (2005). "Nitrogen fixation by Trichodesmium spp.: An important source of new nitrogen to the tropical and subtropical North Atlantic Ocean." Global Biogeochemical Cycles **19**.

Carpenter, E. J., J. P. Montoya, et al. (1999). "Extensive bloom of a N2-fixing diatom/cyanobacterial association in the tropical Atlantic Ocean." Marine Ecology Progress Series **185**: 273-283.

Carpenter, E. J., A. Subramaniam, et al. (2004). "Biomass and primary productivity of the cyanobacterium Trichodesmium spp. in the tropical N Atlantic ocean." Deep-Sea Research Part I-Oceanographic Research Papers **51**(2): 173-203.

Cooley, S. R. and P. L. Yager (2006). "Physical and biological contributions to the western tropical North Atlantic Ocean carbon sink formed by the Amazon River plume." Journal of Geophysical Research-Oceans **111**(C8).

Demaster, D. J. and R. H. Pope (1996). "Nutrient dynamics in Amazon shelf waters: Results from AMASSEDS." Continental Shelf Research **16**(3): 263-289.

Eppley, R. and B. Peterson (1979). "Particulate Organic-Matter Flux and Planktonic New Production In the Deep Ocean." Nature **282**: 667-680.

Foster, R. A., A. Subramaniam, et al. (2007). "Influence of the Amazon River plume on distributions of free-living and symbiotic cyanobacteria in the western tropical north Atlantic Ocean." Limnology and Oceanography **52**(2): 517-532.

Foster, R. A., A. Subramaniam, et al. (2009). "Distribution and activity of diazotrophs in the Eastern Equatorial Atlantic." Environmental microbiology **11**(4): 741-750.

Fox, L. E., S. L. Sager, et al. (1986). "The chemical control of soluble phosphorus in the Amazon estuary." Geochimica Et Cosmochimica Acta **50**(5): 783-794.

Goericke, R., J. P. Montoya, et al. (1994). Physiology of isotope fractionation in algae and cyanobacteria. Stable Isotopes in Ecology and Environmental Science. K. Lajtha and B. Michener. Oxford, Blackwell Scientific Publications**:** 187-221.

Goes, J. I., H. d. R. Gomes, et al. (Submitted). "Biogeography of Phytoplankton Communities in the Western Tropical North Atlantic as Influenced by Discharge from the Amazon River."

Gruber, N. and J. L. Sarmiento (2002). "Large-Scale Biogeochemical-Physical Interactions In Elemental Cycles." The sea **12**.

Hawser, S. P., J. M. Oneil, et al. (1992). "Toxicity of Blooms of the Cyanobacterium Trichodesmium to Zooplankton." Journal of Applied Phycology **4**(1): 79-86.

Johnson, K. M., A. G. Dickson, et al. (1998). "Coulometric total carbon dioxide analysis for marine studies: assessment of the quality of total inorganic carbon measurements made during the US Indian Ocean CO2 Survey 1994-1996." Marine Chemistry **63**(1-2): 21-37.

Johnson, K. M., K. D. Wills, et al. (1993). "Coulometric Total Carbon-Dioxide Analysis for Marine Studies - Maximizing the Performance of an Automated Gas Extraction System and Coulometric Detector." Marine Chemistry **44**(2-4): 167-187.

Laws, E. A., B. N. Popp, et al. (1995). "Dependence of phytoplankton carbon isotopic composition on growth rate and $[CO_2]_{aq}$: Theoretical considerations and experimental results." Geochimica et Cosmochimica Acta **59**: 1131-1138.

Lohrenz, S. E., G. L. Fahnenstiel, et al. (1997). "Variations in primary production of northern Gulf of Mexico continental shelf waters linked to nutrient inputs from the Mississippi River." Marine Ecology-Progress Series **155**: 45-54.

Longhurst, A. (1993). "Seasonal cooling and blooming in tropical oceans." Deep Sea Research Part I: Oceanographic Research **40**: 2145-2165.

Mikaloff Fletcher, S. E., N. Gruber, et al. (2007). "Inverse estimates of the oceanic sources and sinks of natural CO2 and the implied oceanic carbon transport." Global Biogeochemical Cycles **21**: 1-19.

Montoya, J. P. (2008). Nitrogen stable isotopes in marine environments. Nitrogen in the Marine Environment. D. G. Capone, E. J. Carpenter, M. R. Mulholland and D. A. Bronk, Academic press**:** 1277-1302.

Montoya, J. P., E. J. Carpenter, et al. (2002). "Nitrogen fixation and nitrogen isotope abundances in zooplankton of the oligotrophic North Atlantic." Limnology and Oceanography **47**(6): 1617-1628.

Muller-Karger, F. E., P. L. Richardson, et al. (1995). "On the offshore dispersal of the Amazon ' s Plume in the North Atlantic : Comments on the paper by A . Longhurst , " Seasonal cooling and blooming in tropical oceans "." Deep Sea Research Part I: Oceanographic Research Papers **42**: 2127-2137.

Rau, G. H., U. Riebesell, et al. (1996). "A model of photosynthetic ^{13}C fractionation by marine phytoplankton based on diffusive molecular CO_2 uptake." Marine Ecology Progress Series **133**: 275-285.

Sigman, D. M., M. A. Altabet, et al. (2000). "The delta N-15 of nitrate in the Southern Ocean: Nitrogen cycling and circulation in the ocean interior." Journal of Geophysical Research-Oceans **105**(C8): 19599-19614.

Smith, W. O. and D. J. Demaster (1996). "Phytoplankton biomass and productivity in the Amazon River plume: Correlation with seasonal river discharge." Continental Shelf Research **16**(3): 291-319.

Smith, W. O. and G. J. Russell (1995). "Phytoplankton biomass and nutrient distributions in the Amazon river plume: Environmental correlates." Geo-Marine Letters **15**(3-4): 195-198.

Subramaniam, A., P. L. Yager, et al. (2008). "Amazon River enhances diazotrophy and carbon sequestration in the tropical North Atlantic Ocean." Proceedings of the National Academy of Sciences of the United States of America **105**: 10460-10465.

Sweeney, C., D. A. Hansell, et al. (2000). "Biogeochemical regimes, net community production and carbon export in the Ross Sea, Antarctica." Deep-Sea Research Part Ii-Topical Studies in Oceanography **47**(15-16): 3369-3394.

Takahashi, T., S. C. Sutherland, et al. (2002). "Global sea – air CO2 flux based on climatological surface ocean pCO2 , and seasonal biological and temperature effects." Deep Sea Research Part II: Topical Studies in Oceanography **49**: 1601-1622.

Villareal, T. A. (1989). "Division Cycles in the Nitrogen-Fixing Rhizosolenia (Bacillariophyceae) Richelia (Nostocaceae) Symbiosis." British Phycological Journal **24**(4): 357-365.

Villareal, T. A. (1990). "Laboratory Culture and Preliminary Characterization of the Nitrogen-Fixing Rhizosolenia-Richelia Symbiosis." Marine Ecology-Pubblicazioni Della Stazione Zoologica Di Napoli I **11**(2): 117-132.

Vorosmarty, C., B. Fekete, et al. (2000). "Global system of rivers: Its role in organizing continental land mass and defining land-to-ocean linkages." Global Biogeochemical **14**: 599-621.

Voss, M., D. Bombar, et al. (2006). "Riverine influence on nitrogen fixation in the upwelling region off Vietnam, South China Sea." Geophysical Research Letters **33**(7).

Yeung, L. Y., W. M. Berelson, et al. (2012). "Impact of diatom-diazotroph associations on carbon export in the Amazon River plume." Geophysical Research Letters **39**: 1-6.

Tables

Table 1 – End-member salinity and nutrient concentrations (mean ± SE) used to calculate conservative mixing relationships. River and oceanic end-member values (N = 6 each) were from samples at the lowest measured salinity and from oceanic stations to the SE, outside of the plume influence.

End-Member	Salinity (psu)	PO_4^{3-} (μM)	SiO_2 (μM)
River	17.95 ± 0.61	0.53 ± 0.04	50.0 ± 3.39
Oceanic	35.62 ± 0.24	0.03 ± 0.04	1.13 ± 0.73

Figure Legends

Figure 1 – (a) Cruise track of R/V Knorr cruise KN197-8 in summer 2010 off the northeastern coast of South America. (b) Composite of MODIS-Aqua chlorophyll *a* images for the period of the cruise. (c) Composite of kd490 satellite images for the period of the cruise.

Figure 2 – Surface distributions of salinity (a, c) and chlorophyll a (b, d) from legs 1 (a, b) and 2 (c, d) of cruise KN197-8.

Figure 3 – Concentrations of nitrate (a), phosphate (b), and silicate (c) as a function of salinity. Red lines in (b) and (c) reflect conservative mixing of plume and oceanic end members and were calculated using nutrient concentrations from the lowest measured salinity (16.6 psu) and from offshore oceanic stations (35.6 psu) SE of the plume. Vertical dotted lines separate the low salinity, mesohaline, and oceanic salinity regions.

Figure 4 – Surface distributions of salinity (a), NO_3^- (b), PO_4^{3-} (c), and SiO_2 (d). Panels (e) and (f) show deviations from conservative mixing of PO_4^{3-} and SiO_2, respectively.

Figure 5 – Surface distributions of salinity (a), C:N ratios (b), and particulate carbon (c) and nitrogen (d) concentrations.

Figure 6 – (a) Abundances of *Trichodesmium spp.*, *R. clevei*, and *H. hauckii* as a function of salinity. The maximum abundance of *H. hauckii* (965,708 Cells L^{-1}) is off scale. $\delta^{13}C$ (b) and $\delta^{15}N$ (c) of particles as a function of salinity from underway and surface CTD samples. The green and blue lines in (c) designate the average $\delta^{15}N$ of riverine organic N and deep NO_3^- (5‰; Sigman et al. 2000), and diazotrophic biomass (-2‰; Montoya et al. 2002), respectively. Salinity regions are separated by vertical dotted lines as in Fig. 3.

Figure 7 – Surface distributions of salinity (a), $\delta^{13}C$ (b), $\delta^{15}N$ (c), and % N_D (diazotrophic contribution to particulate nitrogen; d).

Figure 8 – Surface distributions of salinity (a) and abundances of *Trichodesmium* spp. (b), *H. hauckii* (c), *R. clevei* (d).

Figure 9 – Distributions of scaled-ΔpCO_2 (a) and $\Delta DIC_{BIO,INT}$ (b). ΔpCO_2 was scaled to plume thickness using a plume thickness factor (ptf): $S < 25$, ptf = 1; $25 \leq S < 30$, ptf = 1.5; $30 \leq S < 35$, ptf = 3; $S \geq 35$, ptf = 5. $\Delta DIC_{BIO,INT}$ represents ΔDIC_{BIO} integrated through the plume layer.

Figure 10 – % N_D (diazotrophic contribution to particulate nitrogen) as a function of *Trichodesmium* spp. (left) and *H. hauckii* (right) abundance.

Figure 1

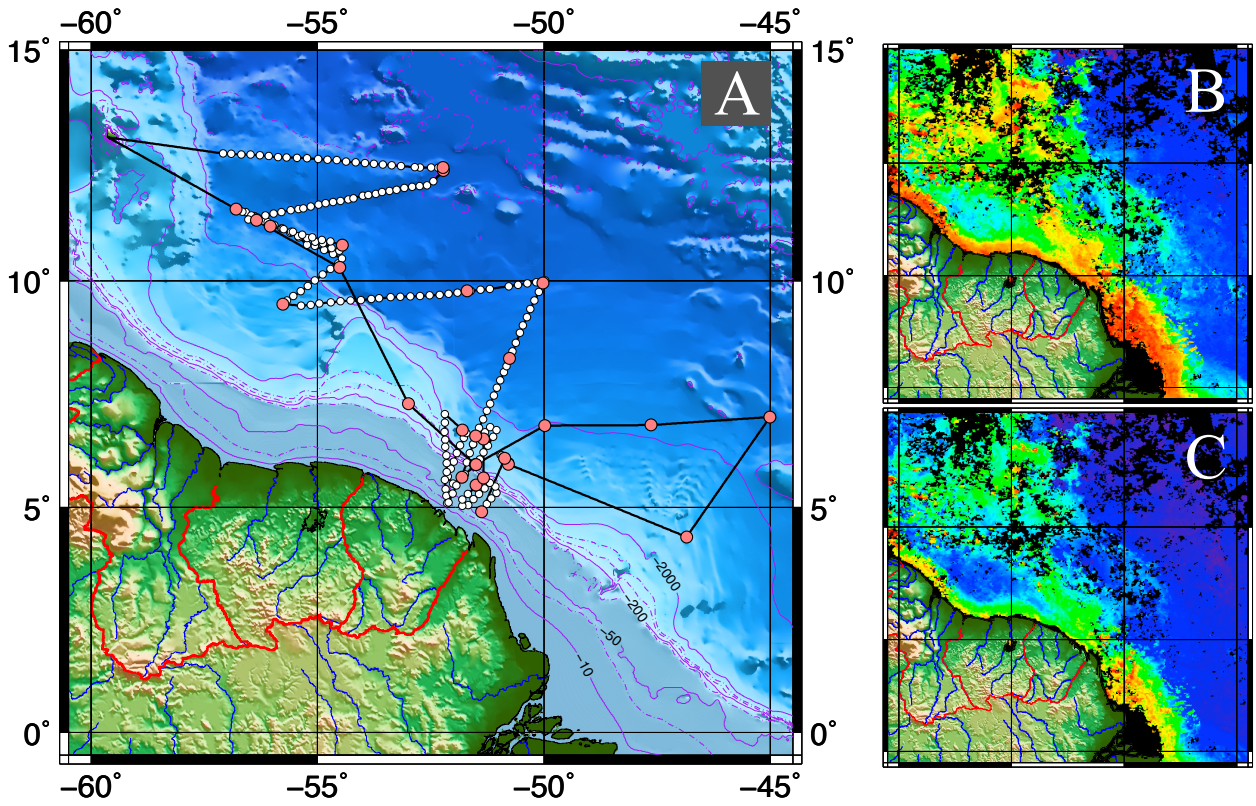

Figure 2

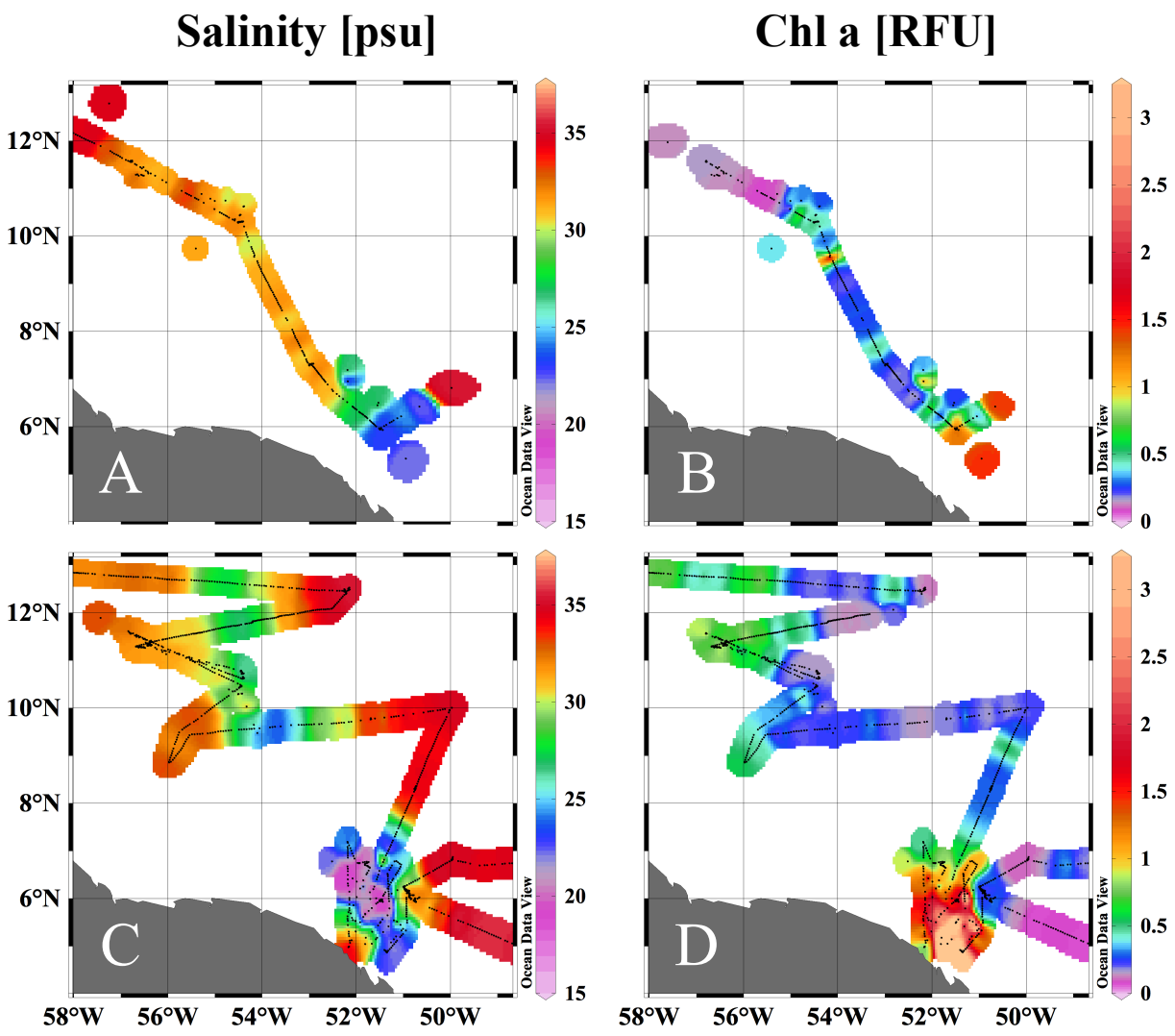
Salinity [psu]
Chl a [RFU]
A
B
C
D
12°N
10°N
8°N
6°N
58°W
56°W
54°W
52°W
50°W
35
30
25
20
15
3
2.5
2
1.5
1
0.5
0
Ocean Data View

1 **Figure 3**

2

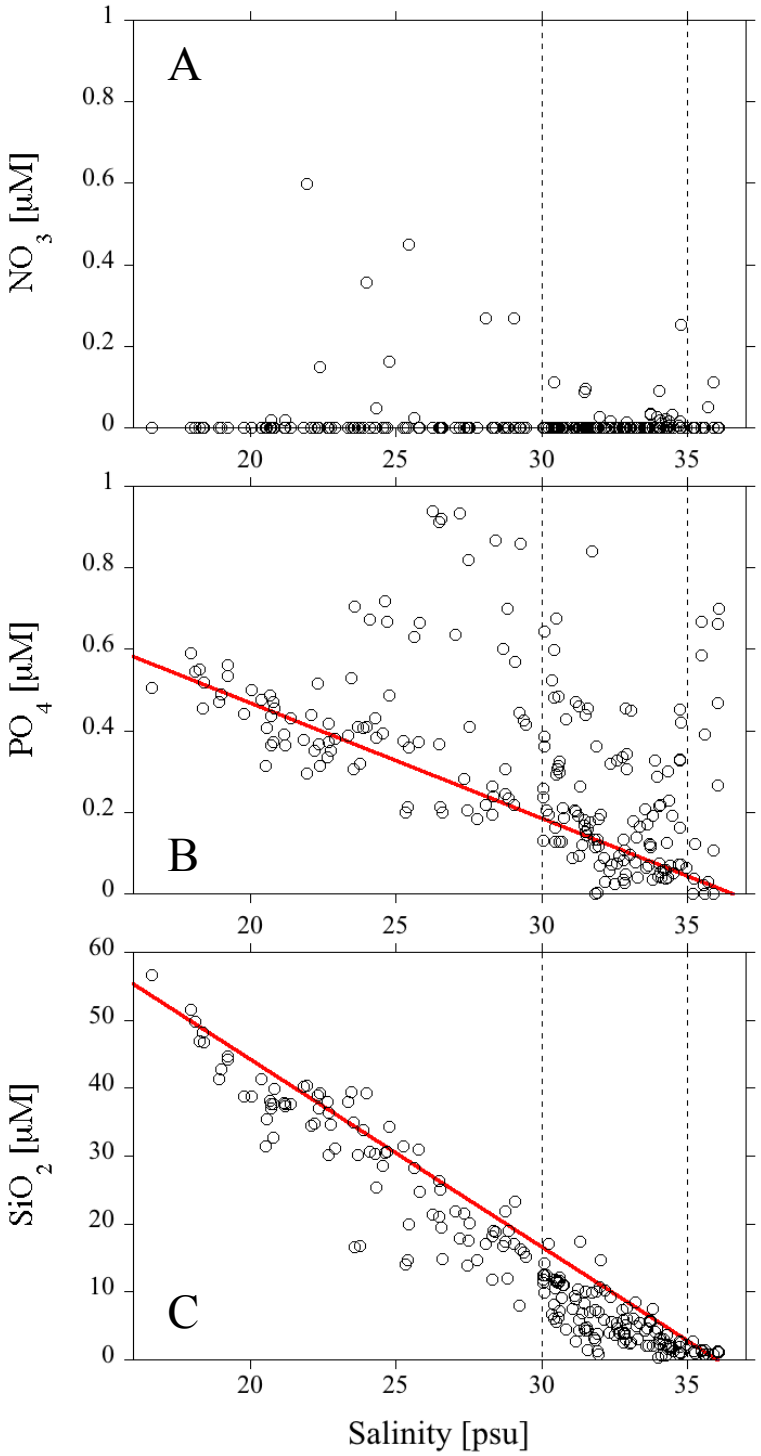
A
B
C
NO3 [µM]
PO4 [µM]
SiO2 [µM]
Salinity [psu]
0
0.2
0.4
0.6
0.8
1
10
20
30
40
50
60
20
25
30
35

1

Figure 4

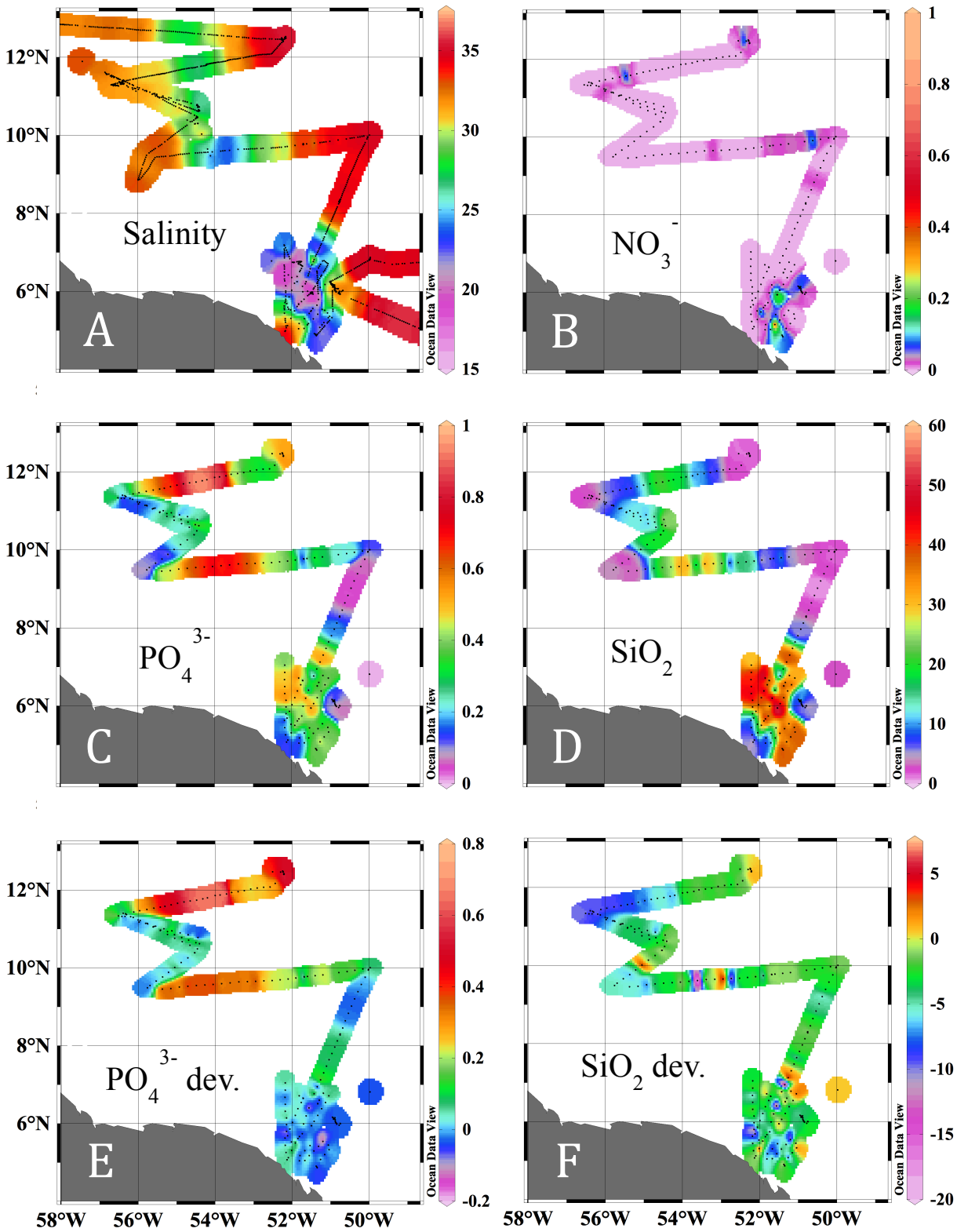
12°N
10°N
8°N
6°N
Salinity
A
35
30
25
20
15
Ocean Data View
NO_3^-
B
1
0.8
0.6
0.4
0.2
0
PO_4^{3-}
C
SiO_2
D
60
50
40
30
20
10
PO_4^{3-} dev.
E
0.8
0.6
0.4
0.2
0
-0.2
SiO_2 dev.
F
5
0
-5
-10
-15
-20
58°W
56°W
54°W
52°W
50°W

Figure 5

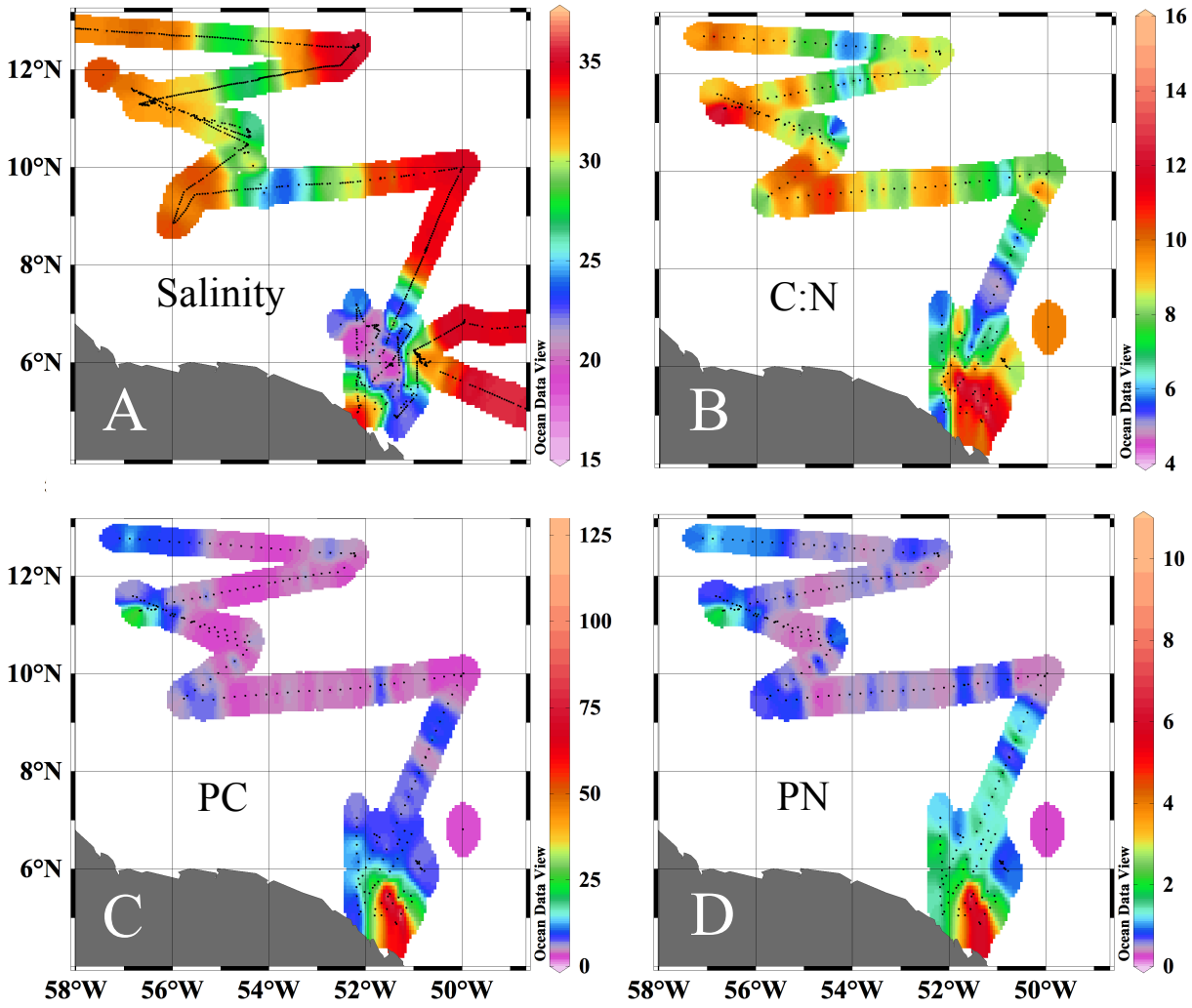
12°N
10°N
8°N
6°N
Salinity
A
35
30
25
20
15
Ocean Data View
C:N
B
16
14
12
10
8
6
4
PC
C
125
100
75
50
25
0
PN
D
10
8
6
4
2
0
58°W
56°W
54°W
52°W
50°W

1 **Figure 6**

2

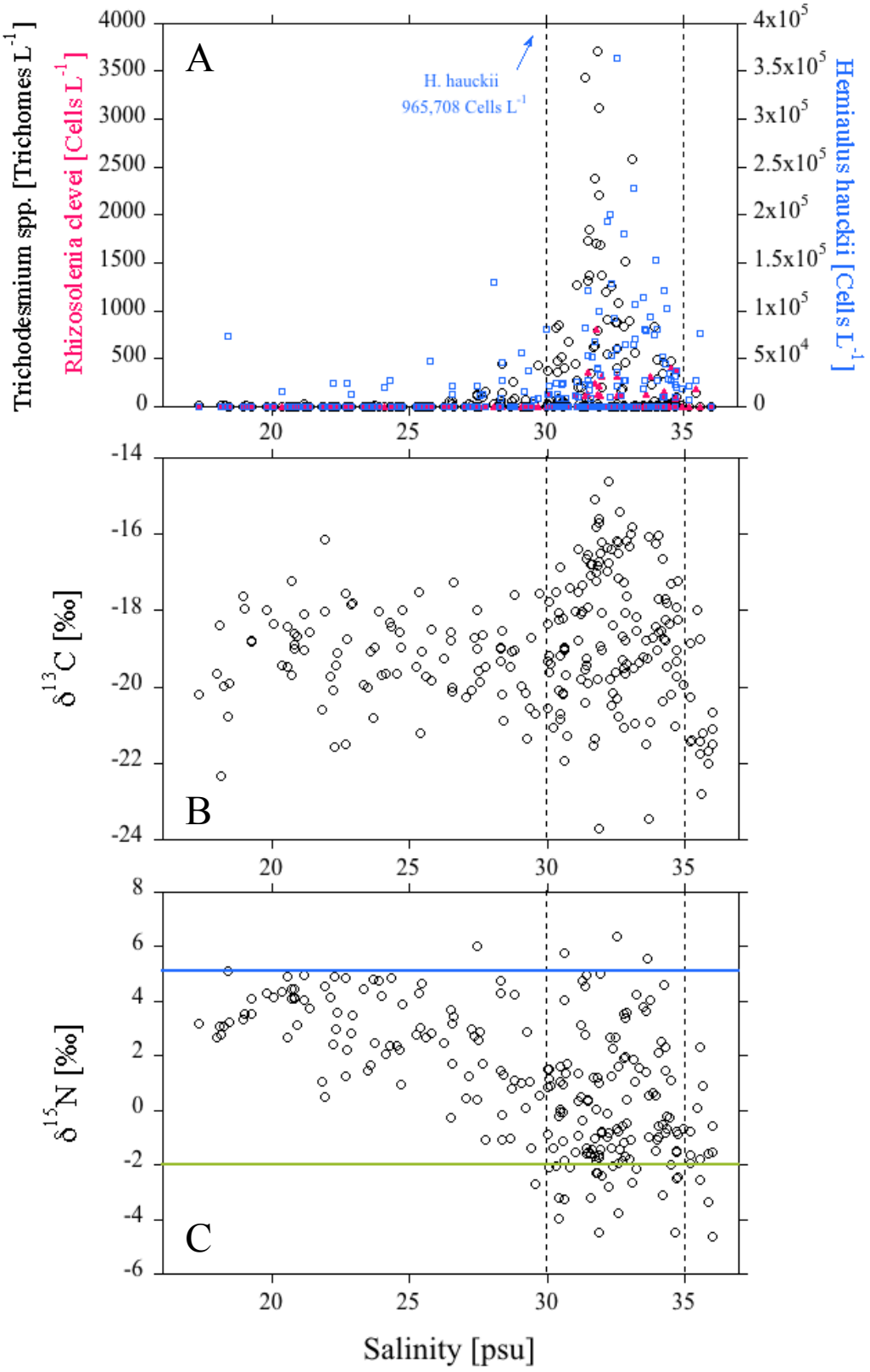
A
B
C
Trichodesmium spp. [Trichomes L-1]
Rhizosolenia clevei [Cells L-1]
Hemiaulus hauckii [Cells L-1]
H. hauckii
965,708 Cells L-1
δ13C [‰]
δ15N [‰]
Salinity [psu]

Figure 7

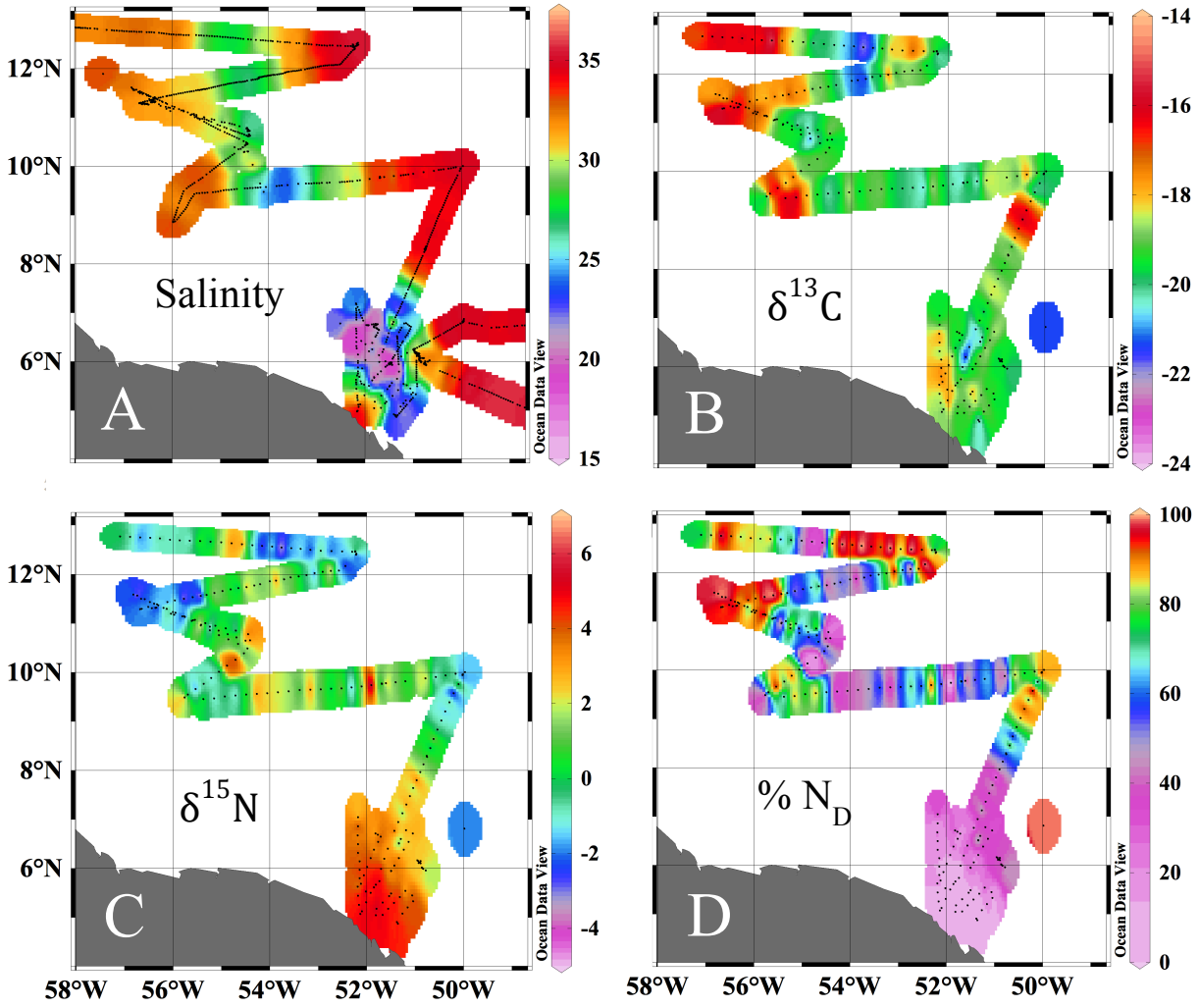
12°N
10°N
8°N
6°N
Salinity
A
35
30
25
20
15
Ocean Data View
δ13C
B
-14
-16
-18
-20
-22
-24
δ15N
C
6
4
2
0
-2
-4
% ND
D
100
80
60
40
20
0
58°W
56°W
54°W
52°W
50°W

Figure 8

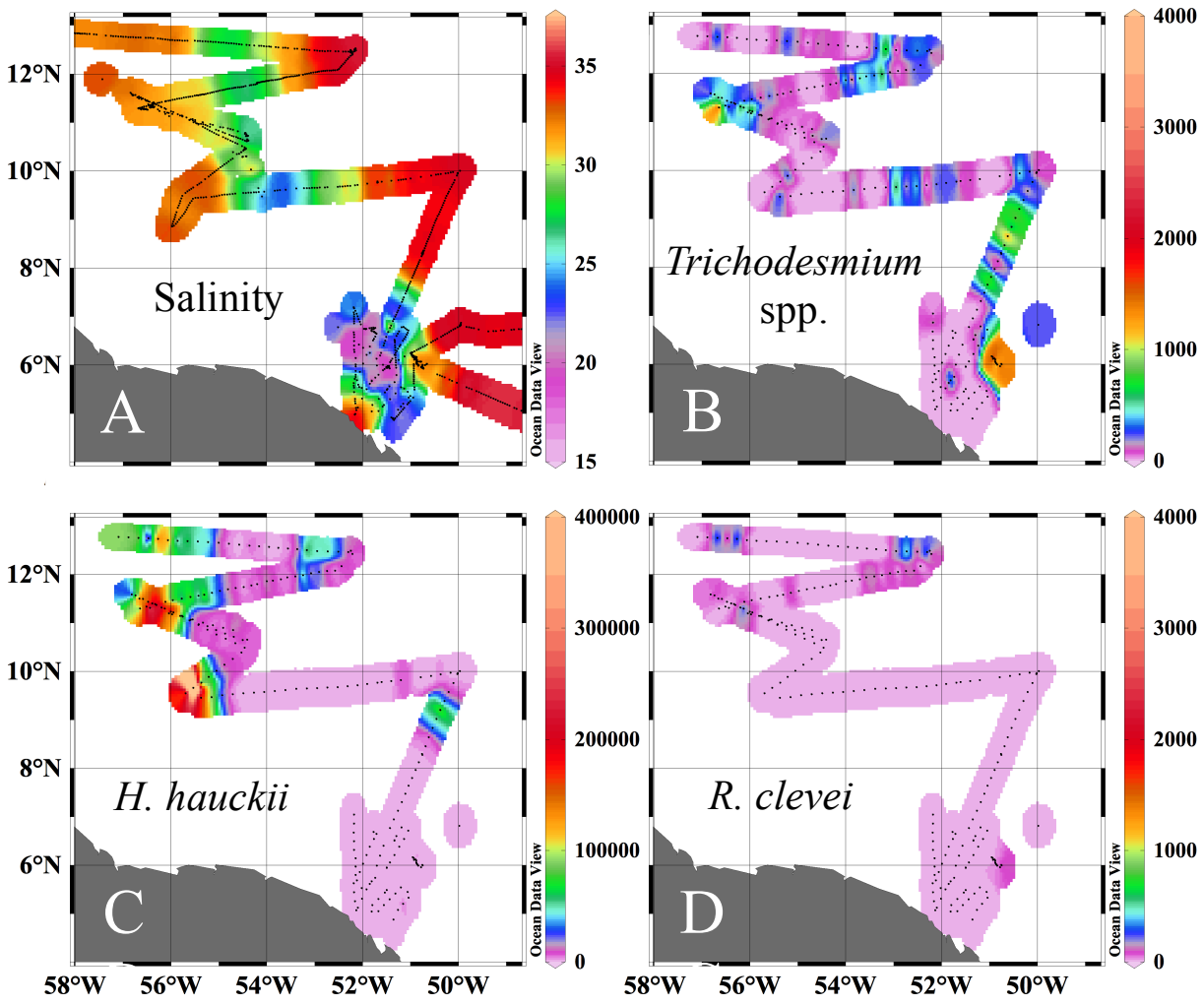
12°N
10°N
8°N
6°N
Salinity
A
35
30
25
20
15
Ocean Data View
Trichodesmium
spp.
B
4000
3000
2000
1000
0
H. hauckii
C
400000
300000
200000
100000
0
R. clevei
D
58°W
56°W
54°W
52°W
50°W

Figure 9

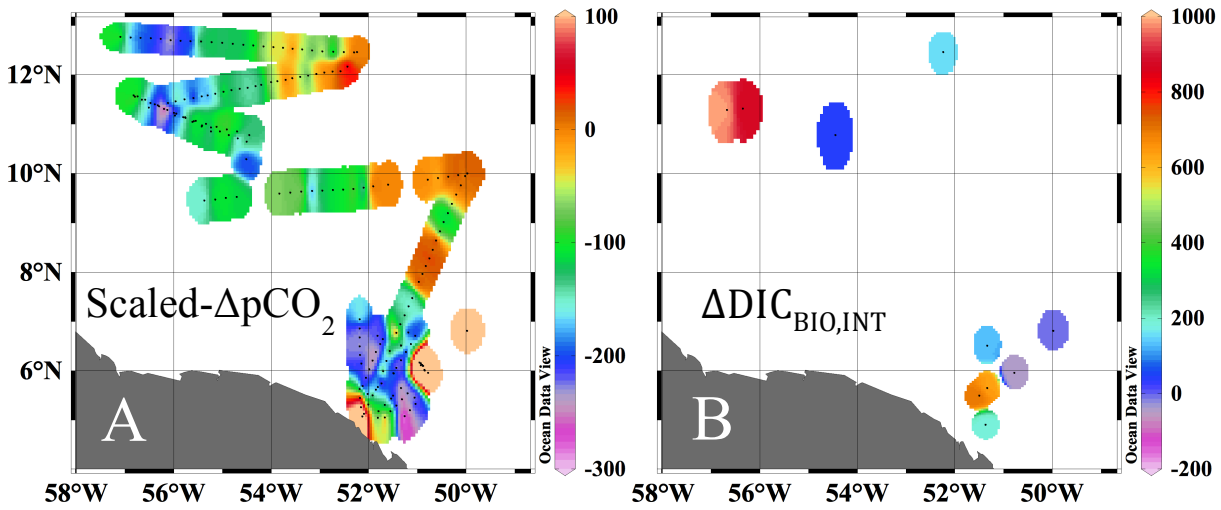
12°N
10°N
8°N
6°N
58°W
56°W
54°W
52°W
50°W
Scaled-ΔpCO2
A
100
0
-100
-200
-300
Ocean Data View
ΔDICBIO,INT
B
1000
800
600
400
200
0
-200
Ocean Data View

1

Figure 10

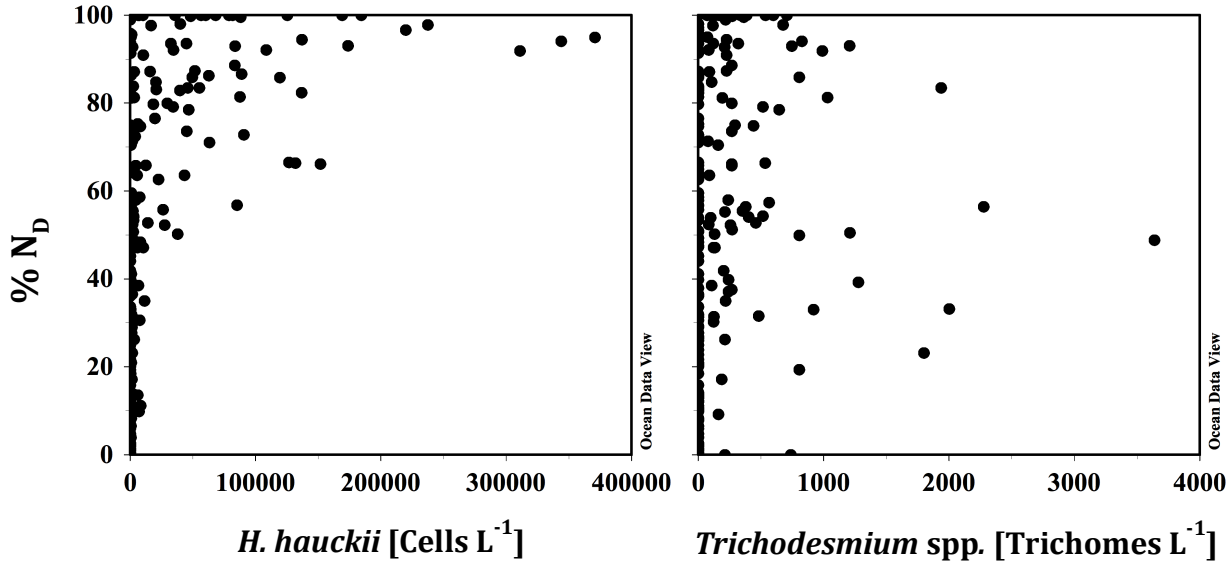
% N_D
100
80
60
40
20
0
0
100000
200000
300000
400000
Ocean Data View
H. hauckii [Cells L^{-1}]
0
1000
2000
3000
4000
Ocean Data View
Trichodesmium spp. [Trichomes L^{-1}]

2